SCIENTIFIC REPORTS
natureresearch

Check for updates

OPEN

A general method for analyzing arbitrary planar negative-refractive-index multilayer slab optical waveguide structures

Yaw-Dong Wu

In this paper, a general method for analyzing arbitrary planar negative-refractive-index (NRI) multilayer slab optical waveguide structures was proposed. Some degenerated examples were introduced to prove the accuracy of the proposed method. The analytical and numerical results show excellent agreement. The method can also be degenerated to analyze arbitrary planar conventional optical waveguide structures. Based on this general method, the analysis and calculation of any kinds of planar NRI slab optical waveguide structures and planar conventional optical waveguide structures can be achieved easily.

The left-handed material with double-negative media ($\varepsilon < 0$, $\mu < 0$) is different from the right-handed material with double-positive media ($\varepsilon > 0$, $\mu > 0$). It has been proposed theoretically and experimentally by Veselago and Shelby et al., respectively[1,2]. The NRI media possess simultaneously the negative dielectric permittivity and permeability[3,4]. Therefore, the NRI media is different from right-handed material with double-negative media. Recently, metamaterial has attracted a lot of attention[5–14]. Many applications of metamaterial have been proposed in various fields, such as antennas, perfect absorber, super lens, invisibility cloaks, optical sensors, phase modulators, and phase holography[5,15–33]. Some numerical and experimental results of metamaterial have also been proposed[34–40]. In the past, all–optical devices based on the conventional nonlinear optical waveguide structures have been proposed, since the spatial solitons can propagate a long distance without changing their spatial shapes[41–46]. In the past, most papers just focused on the study of the properties at the interface between the right-handed material and the metamaterial[47–53]. The TE/TM surface polarizations propagating along the interface between a linear metamaterial and different types of conventional right-handed material were studied. The three-layer metamaterail waveguide with linear cladding and substrate had been discussed[54,55]. In our previous work[56], we proposed a special case of the NRI multilayer slab optical waveguide structures with only the Kerr-type nonlinear cladding. The analyzed processes of the proposed structure are relatively simple compared to that of this manuscript. When all layers of the proposed NRI slab optical waveguide structure are the Kerr-type nonlinear media, the analyses processes will become very complicated and difficult. The difficulty lies in the derivation of the mathematical model and the verification of numerical analyses and simulations. To the best of my knowledge, a general method for analyzing arbitrary NRI slab optical waveguide structures has not been proposed before. This paper gives detailed modal analyses of TE-polarized waves in the NRI multilayer slab waveguide structure with all Kerr-type nonlinear layers. The theoretical results and the numerical results show excellent agreement. The method can also be used to investigate and to analyze the distribution of TE electrical field in the Kerr-type nonlinear NRI multilayer slab optical waveguide structures. To prove the accuracy of the proposed general method for analyzing arbitrary NRI multilayer slab optical waveguide structures, a theoretically degenerated example was introduced. Therefore, the method can provide simultaneously to analyze two different kinds of waveguide structures. One is the nonlinear NRI multilayer slab optical waveguide structure and the other is the linear NRI multilayer slab optical waveguide structure. Based on this general method, the analysis and calculation of any kinds of NRI multilayer slab optical waveguide structures can be achieved easily.

Electronic Engineering Department, National Kaohsiung University of Science and Technology, Kaohsiung, Taiwan. email: ydwu@nkust.edu.tw
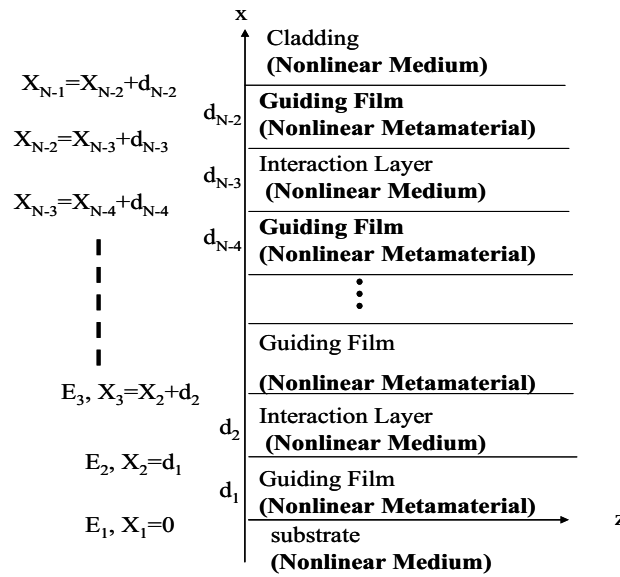
Figure 1. The proposed NRI multilayer slab optical waveguide structure with all Kerr-type nonlinear layers.

Analysis

In general, a transfer matrix approach[57] can be used to analyze the conventional multilayer slab optical waveguide structures. However, it cannot be used to analyze the case of the NRI multilayer slab optical waveguide structure with all Kerr-type nonlinear layers, proposed in this manuscript. When all layers of the proposed NRI slab optical waveguide structure are the Kerr-type nonlinear media, the analytical solutions are very complicated because they contain the Jacobian elliptic functions. It is very difficult to obtain the exact solutions. In this paper, the modal theory[58] was used to derive the formulae of the electric field distributions of the proposed NRI multilayer slab optical waveguide structure with all Kerr-type nonlinear layers, as shown in Fig. 1. The multilayer optical waveguide structure is composed of the guiding films ((N−1)/layers), the interaction layers ((N − 3)/2layers), the cladding layer, and the substrate layer. The total number of layers is N (N = 3, 5, 7,…). The d_j and n_j are used to denote the width and the refractive index of the jth layer, respectively. The nonlinear cladding and substrate layer are assumed to extend to infinity in the + x and − x directions, respectively. The major significance of this assumption is that there are no reflections in the x direction to be concerned with, expect for those occurring at interfaces. For the simplicity, the TE waves are choosing to propagate along the z direction. The wave equation in the j-th layer can be written as:

$$\nabla^2 E_{yj} = \frac{n_j^2}{c^2}\frac{\partial^2 E_{yj}}{\partial t^2} , \ j = 0, 1, 2, \ldots, N-1 \tag{1}$$

with the solutions of the form:

$$E_{yj}(x, z, t) = E_j(x)\exp[i(\omega t - \beta k_o z)] \tag{2}$$

where β is the effective refractive index, ω is the angular frequency, and k_0 is the wave number in the free space. For the Kerr-type nonlinear medium, the square of the refractive index n_j^2 in the nonlinear NRI slab guiding films, nonlinear interaction layer, nonlinear cladding, and nonlinear substrate can be expressed as[48]:

$$n_j^2 = \varepsilon_j\mu_j + \alpha_j\left|E_j(x)\right|^2, \ j = 0, 1, 2, \ldots, N-1 \tag{3}$$

where ε_j and μ_j (j = 1, 3,…, N − 2) are the negative dielectric permittivity and permeability in the nonlinear NRI slab guiding layer, respectively, and The rest layers are the positive dielectric permittivity and permeability. The α_j is the nonlinear coefficient of the j-th layer Kerr-type nonlinear medium. By substituting Eqs. (2) and (3) into the wave equation Eq. (1), the transverse electric fields can be solved in each layer. The transverse electric fields in each layer can be expressed as:

$$\left[\frac{d^2}{dx^2} + q_j^2 + \alpha_j k_0^2\left|E_j^2(x)\right|\right]E_j(x) = 0 , \text{ for j} = \text{N} - 1, \text{ in the nonlinear cladding} \tag{4}$$

$$\left[\frac{d^2}{dx^2} + q_j^2 + \alpha_j k_0^2\left|E_j^2(x)\right|\right]E_j(x) = 0,$$

for $j = 1, 2, 3 \ldots N − 2$, in the nonlinear NRI slab guiding films and the nonlinear interaction layers
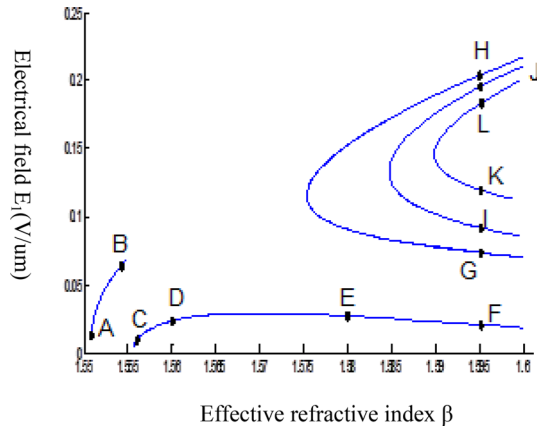
$$\tag{5}$$

Figure 2. Dispersion curve of the proposed five-layer all Kerr-type nonlinear NRI slab optical waveguide structure with constants: $d_f = d_1 = d_3 = 5$ μm and $d_i = d_2 = 3$ μm.

$$\left[\frac{d^2}{dx^2} + q_j^2 + \alpha_j k_0^2 \left|E_j^2(x)\right|\right] E_j(x) = 0, \text{ for } j = 0, \text{ in the nonlinear substrate} \tag{6}$$

$$q_j^2 = k_0^2\left(\varepsilon_j\mu_j - \beta^2\right), \text{ for } \beta < \varepsilon_j\mu_j \text{ and } j = 0, 1, 2, 3 \ldots N - 1 \tag{7}$$

$$q_j^2 = Q_j^2 = -k_0^2\left(\varepsilon_j\mu_j - \beta^2\right), \text{for } \beta > \varepsilon_j\mu_j \text{ and } j = 1, 3, 5 \ldots N - 1 \tag{8}$$

By matching the boundary conditions, the solutions of electric fields in the nonlinear NRI slab guiding films and the nonlinear interaction layers can be written as:

$$E_j(x) = b_j cn\left[A_j\left(x + x_j\right)\big|m_j\right],$$
$$\text{for } j = 1, 2, 3, \ldots, N - 2, \text{ in the nonlinearNRIslabguidingfilmsandthenonlinear interactionlayers} \tag{9}$$

The parameters A_j, m_j, x_j, a_j^2, and b_j^2 can be expressed as:

$$A_j = [q_j^4 + 2\alpha_j k_0^2 K_j]^{1/4}, \quad m_j = \frac{b_j^2}{a_j^2 + b_j^2}, \quad x_j = cn^{-1}\left(\frac{E_j}{b_j}\right), \quad a_j^2 = \frac{\sqrt{q_j^4 + 2\alpha_j k_0^2 K_j} + q_j^2}{\alpha_j k_0^2}, \quad b_j^2 = \frac{\sqrt{q_j^4 + 2\alpha_j k_0^2 K_j} - q_j^2}{\alpha_j k_0^2} \tag{10}$$

where cn is a specific Jacobian elliptic function, m_j is the modulus, and x_j is the second constants of integration. By solving the differential Eqs. (4) and (6), the transverse electric fields in the Kerr-type nonlinear cladding and in the Kerr-type nonlinear substrate can be expressed as follows:

$$E_j(x) = E_j\left\{\cosh[q_j\left(x - x_j\right)] + B_c \sinh[q_j\left(x - x_j\right))]\right\}^{-1}, \text{ for } j = N - 1 \tag{11}$$

$$E_0(x) = E_1\left\{\cosh(q_0 x) - B_s \sinh(q_0 x)\right\}^{-1} \tag{12}$$

where B_c and B_s can be expressed as:

$$B_c = \sqrt{1 - \frac{\alpha_{N-1}E_{N-1}}{2q_{N-1}^2}}, \quad B_s = \sqrt{1 - \frac{\alpha_0 E_1}{2q_0^2}} \tag{13}$$

The parameters E_1 and E_{N-1} are the values of the electric fields at the lowest and uppermost boundaries of the nonlinear NRI slab guiding films, respectively. By matching the boundary conditions, the dispersion equation can be written as:

$$E_j(x) = b_j cn\left[A_j\left(x + x_j\right)\big|m_j\right] = E_{j-1} cn\left[A_j x_j\big|m_j\right]\frac{1 - \frac{sn[A_j x|m_j]dn[A_j x|m_j]}{cn[A_j x|m_j]}\varphi_f\left[A_j x_j\right]}{1 - m_j sn^2\left[A_j x\big|m_j\right] sn^2\left[A_j x_j\big|m_j\right]}, \text{ for } j = 1, 2, 3 \ldots N-2 \tag{14}$$

$$\varphi_f\left[A_1 x_1\right] = \frac{sn[A_1 x_1|m_1]dn[A_1 x_1|m_1]}{cn[A_1 x_1|m_1]} = -\frac{\mu_1 B_s q_0}{\mu_0 A_1} \tag{15}$$
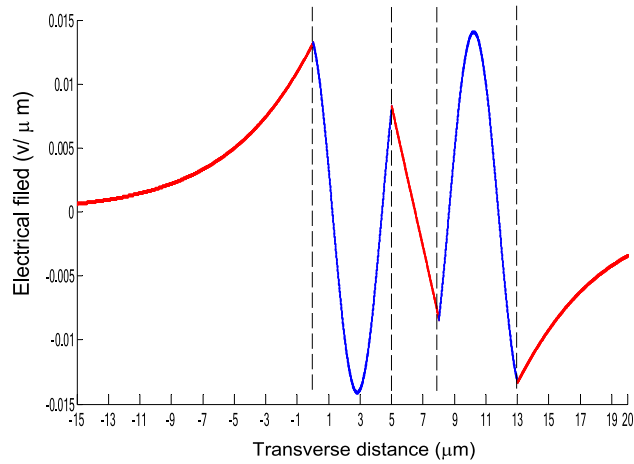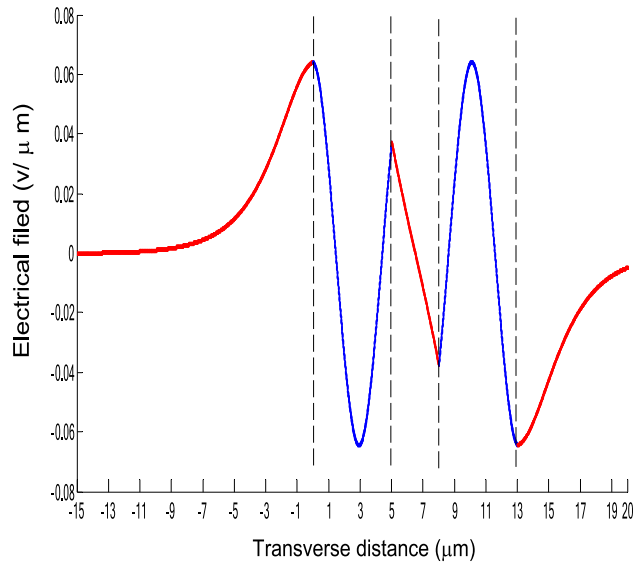
Figure 3. The electrical field distribution of the five-layer all Kerr-type nonlinear NRI slab optical waveguide structure with constants: $\alpha_0 = \alpha_1 = \alpha_2 = \alpha_3 = \alpha_4 = 6.3786 \ \mu m^2/V^2; \mu_f = \mu_1 = \mu_3 = -2$, $d_1 = d_3 = 5 \ \mu m, d_2 = 3 \ \mu m, \varepsilon_f \mu_f = \varepsilon_1 \mu_1 = \varepsilon_3 \mu_3 = 2.4649, \varepsilon_0 \mu_0 = \varepsilon_2 \mu_2 = \varepsilon_4 \mu_4 = 2.4025$, and $\lambda = 1.3 \ \mu m$ with respect to the point A as shown in Fig. 2.

Figure 4. The electrical field distribution of the five-layer all Kerr-type nonlinear NRI slab optical waveguide structure with constants: $\alpha_0 = \alpha_1 = \alpha_2 = \alpha_3 = \alpha_4 = 6.3786 \ \mu m^2/V^2, \mu_f = \mu_1 = \mu_3 = -2$, $d_1 = d_3 = 5 \ \mu m, d_2 = 3 \ \mu m, \varepsilon_f \mu_f = \varepsilon_1 \mu_1 = \varepsilon_3 \mu_3 = 2.4649, \varepsilon_0 \mu_0 = \varepsilon_2 \mu_2 = \varepsilon_4 \mu_4 = 2.4025$, and $\lambda = 1.3 \ \mu m$ with respect to the pointB as shown in Fig. 2.

$$\frac{\mu_j A_{j+1}}{\mu_{j+1} A_j} = \frac{\varphi_f [A_j d_j + A_j x_j | m_j]}{\varphi_f [A_{j+1} x_{j+1} | m_{j+1}]}, \quad \text{for } j = 1, 2, 3 \ldots \text{ N} - 3 \tag{16}$$

$$\frac{B_c q_{N-1} \mu_j}{\mu_{N-1} A_j} = \frac{\varphi_f [A_j d_j] \left\{ dn^2 [A_j x_j | m_j] - m_j sn^2 [A_j x_j | m_j] cn^2 [A_j d_j | m_j] \right\}}{[1 - \varphi_f [A_j d_j] \varphi_f [A_j x_j]] \{1 - m_j sn^2 [A_j d_j | m_j] sn^2 [A_j x_j | m_j]\}}$$
$$+ \frac{\varphi_f [A_j x_j] \left\{ dn^2 [A_j d_j | m_j] - m_j sn^2 [A_j d_j | m_j] cn^2 [A_j x_f | m_j] \right\}}{[1 - \varphi_f [A_j d_j] \varphi_f [A_j x_j]] \left\{ 1 - m_j sn^2 [A_j d_j | m_j] sn^2 [A_j x_j | m_j] \right\}}, \quad \text{for } j = N - 2 \tag{17}$$

$$\varphi_f [A_j d_j] = \frac{sn [A_j d_j | m_j] dn [A_j d_j | m_j]}{cn [A_j d_j | m_j]} \tag{18}$$
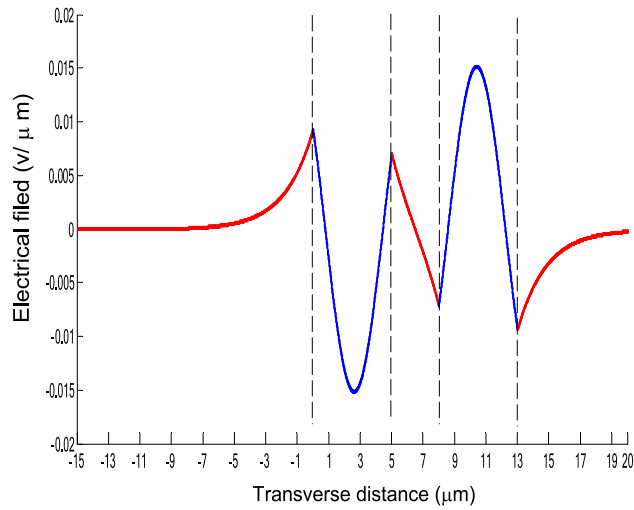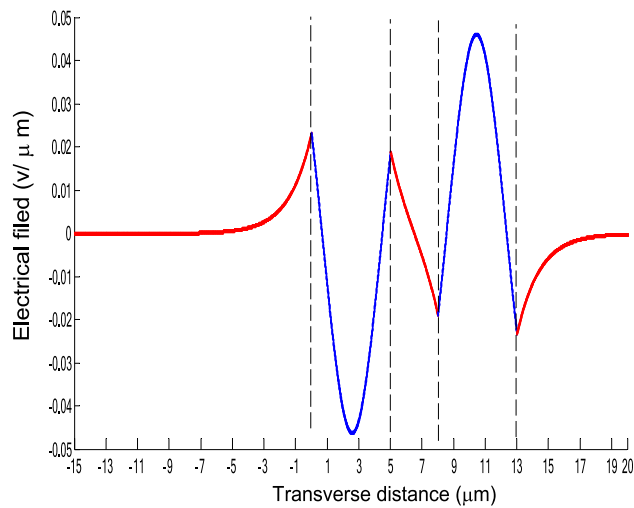
Figure 5. The electrical field distribution of the five-layer all Kerr-type nonlinear NRI slab optical waveguide structure with constants: $\alpha_0 = \alpha_1 = \alpha_2 = \alpha_3 = \alpha_4 = 6.3786$ $\mu m^2/V^2$, $\mu_f = \mu_1 = \mu_3 = -2$, $d_1 = d_3 = 5$ μm, $d_2 = 3$ μm, $\varepsilon_f \mu_f = \varepsilon_1 \mu_1 = \varepsilon_3 \mu_3 = 2.4649$, $\varepsilon_0 \mu_0 = \varepsilon_2 \mu_2 = \varepsilon_4 \mu_4 = 2.4025$, and $\lambda = 1.3$ μm with respect to the point C as shown in Fig. 2.

Figure 6. The electrical field distribution of the five-layer all Kerr-type nonlinear NRI slab optical waveguide structure with constants: $\alpha_0 = \alpha_1 = \alpha_2 = \alpha_3 = \alpha_4 = 6.3786$ $\mu m^2/V^2$, $\mu_f = \mu_1 = \mu_3 = -2$, $d_1 = d_3 = 5$ μm, $d_2 = 3$ μm, $\varepsilon_f \mu_f = \varepsilon_1 \mu_1 = \varepsilon_3 \mu_3 = 2.4649$, $\varepsilon_0 \mu_0 = \varepsilon_2 \mu_2 = \varepsilon_4 \mu_4 = 2.4025$, and $\lambda = 1.3$ μm with respect to the point D as shown in Fig. 2.

$$\varphi_f \left[A_j x_j \right] = \frac{sn \left[A_j x_j \middle| m_j \right] dn \left[A_j x_j \middle| m_j \right]}{cn \left[A_j x_j \middle| m_j \right]} \tag{19}$$

$$
\begin{aligned}
\varphi_f [A_j d_j + A_j x_j | m_j] &= \frac{sn \left[A_j d_j + A_j x_j \middle| m_j \right] dn[A_j d_j + A_j x_j | m_j]}{cn[A_j d_j + A_j x_j | m_j]} \\
&= \frac{\varphi_f [A_j d_j | m_j] \{ dn^2 \left[A_j x_j \middle| m_j \right] - m_j sn^2 \left[A_j x_j \middle| m_j \right] cn^2 [A_j d_j | m_j] \}}{\left\{ 1 - \varphi_f \left[A_j d_j \middle| m_j \right] \varphi_f \left[A_j x_j \middle| m_j \right] \right\} \left\{ 1 - m_j sn^2 \left[A_j d_j \middle| m_j \right] sn^2 \left[A_j x_j \middle| m_j \right] \right\}} \\
&= \frac{\varphi_f [A_j x_j | m_j] \{ dn^2 \left[A_j d_j \middle| m_j \right] - m_j sn^2 \left[A_j d_j \middle| m_j \right] cn^2 [A_j x_j | m_j] \}}{\left\{ 1 - \varphi_f \left[A_j d_j \middle| m_j \right] \varphi_f \left[A_j x_j \middle| m_j \right] \right\} \left\{ 1 - m_j sn^2 \left[A_j d_j \middle| m_j \right] sn^2 \left[A_j x_j \middle| m_j \right] \right\}}
\end{aligned} \tag{20}
$$

where cn, dn, and sn are the Jacobian elliptic functions. Equations (14)–(20) can be solved numerically on a computer. When β and E_1 are determined, all the other constants A_j, m_j, x_j, q_j, Q_j, a_j, and b_j are also determined. The proposed analytic formulas can be used to calculate the transverse electric field function in each
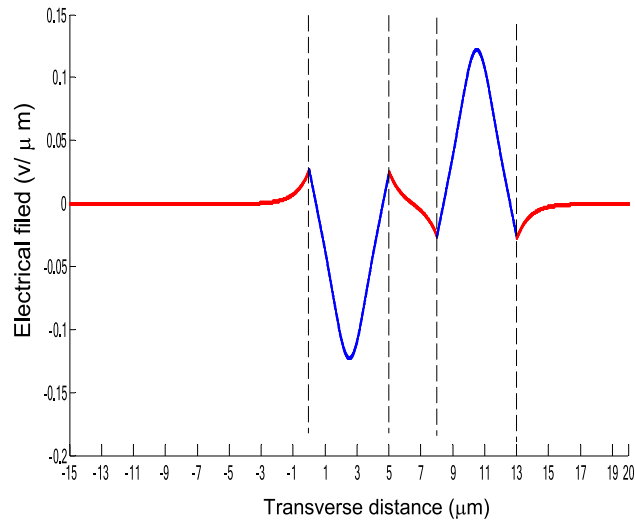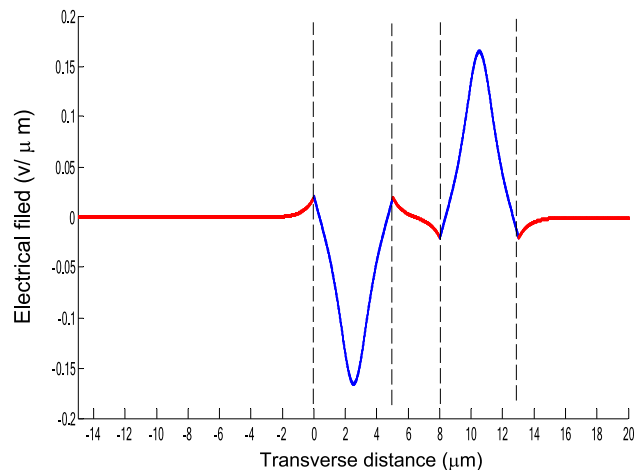
Figure 7. The electrical field distribution of the five-layer all Kerr-type nonlinear NRI slab optical waveguide structure with constants: $\alpha_0 = \alpha_1 = \alpha_2 = \alpha_3 = \alpha_4 = 6.3786$ $\mu m^2/V^2$, $\mu_f = \mu_1 = \mu_3 = -2$, $d_1 = d_3 = 5$ μm, $d_2 = 3$ μm, $\varepsilon_f \mu_f = \varepsilon_1 \mu_1 = \varepsilon_3 \mu_3 = 2.4649$, $\varepsilon_0 \mu_0 = \varepsilon_2 \mu_2 = \varepsilon_4 \mu_4 = 2.4025$, and $\lambda = 1.3$ μm with respect to the point E as shown in Fig. 2.

Figure 8. The electrical field distribution of the five-layer all Kerr-type nonlinear NRI slab optical waveguide structure with constants: $\alpha_0 = \alpha_1 = \alpha_2 = \alpha_3 = \alpha_4 = 6.3786$ $\mu m^2/V^2$, $\mu_f = \mu_1 = \mu_3 = -2$, $d_1 = d_3 = 5$ μm, $d_2 = 3$ μm, $\varepsilon_f \mu_f = \varepsilon_1 \mu_1 = \varepsilon_3 \mu_3 = 2.4649$, $\varepsilon_0 \mu_0 = \varepsilon_2 \mu_2 = \varepsilon_4 \mu_4 = 2.4025$, and $\lambda = 1.3$ μm with respect to the point F as shown in Fig. 2.

layer of the NRI multilayer slab optical waveguide structures. The general formulas can be simplified to analyze five-layer NRI slab optical waveguide structures with all Kerr-type nonlinear layers. Figure 2 shows the dispersion curves of the five-layer all Kerr-type nonlinear NRI slab waveguide structure with the constants: $\alpha_0 = \alpha_1 = \alpha_2 = \alpha_3 = \alpha_4 = 6.3786$ $\mu m^2/V^2$, $\mu_f = \mu_1 = \mu_3 = -2$, $d_1 = d_3 = 5$ μm, $d_2 = 3$ μm, $\varepsilon_f \mu_f = \varepsilon_1 \mu_1 = \varepsilon_3 \mu_3 = 2.4649$, $\varepsilon_0 \mu_0 = \varepsilon_2 \mu_2 = \varepsilon_4 \mu_4 = 2.4025$, and $\lambda = 1.3$ μm. Since there always exist a forbidden region near the effective refractive index β = 1.555 for transverse electric waves in the proposed NRI slab waveguide, the points B and C shown in Fig. 2 are not continue. There are five modes in the proposed five layer NRI slab optical waveguide structures with all Kerr-type nonlinear layers at $d_f = d_1 = d_3 = 5$ μm and $d_i = d_2 = 3$ μm. When the points on the same dispersion curve, it means that they belong to the same mode, with the same unique shapes of each mode. For the conventional linear 5-layer slab waveguide structure, the dispersion curve is linear, and no forbidden region exists. When the width of the guiding film increases, the number of the guiding modes will also increase. The direction of the guided power in the proposed five-layer NRI slab optical waveguide structures with all Kerr-type nonlinear layers is opposed to the conventional linear 5-layer slab waveguide structure. Figures 3, 4, 5, 6, 7, 8, 9, 10, 11, 12, 13 and 14 show the electric field distributions of the proposed five-layer NRI slab optical waveguide structures with all Kerr-type nonlinear layers for several points A-L, as shown in Fig. 2. Figure 3 shows the electrical field distribution with respect to the point A, as shown in Fig. 2. Figure 4 shows
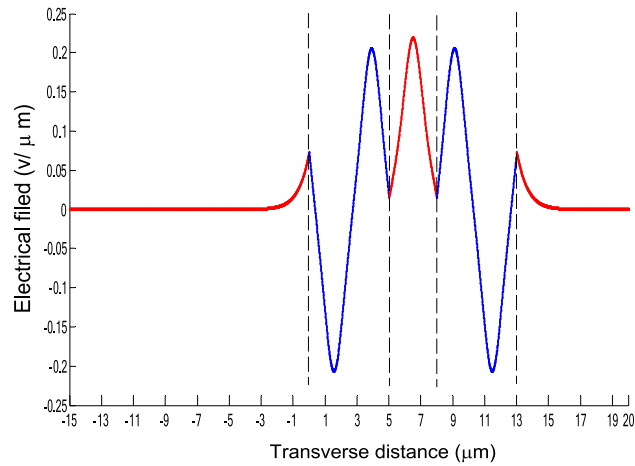
Figure 9. The electrical field distribution of the five-layer all Kerr-type nonlinear metamaterial waveguide with constants: $\alpha_0 = \alpha_1 = \alpha_2 = \alpha_3 = \alpha_4 = 6.3786$ μm^2/V^2, $\mu_f = \mu_1 = \mu_3 = -2$, $d_1 = d_3 = 5$ μm, $d_2 = 3$ μm, $\varepsilon_f\mu_f = \varepsilon_1\mu_1 = \varepsilon_3\mu_3 = 2.4649$, $\varepsilon_0\mu_0 = \varepsilon_2\mu_2 = \varepsilon_4\mu_4 = 2.4025$, and $\lambda = 1.3$ μm with respect to the point G as shown in Fig. 2.
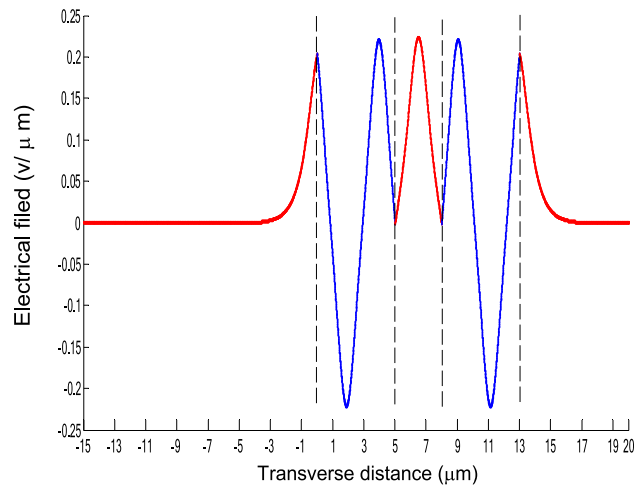

Figure 10. The electrical field distribution of the five-layer all Kerr-type nonlinear NRI slab optical waveguide structure with constants: $\alpha_0 = \alpha_1 = \alpha_2 = \alpha_3 = \alpha_4 = 6.3786$ μm^2/V^2, $\mu_f = \mu_1 = \mu_3 = -2$, $d_1 = d_3 = 5$ μm, $d_2 = 3$ μm, $\varepsilon_f\mu_f = \varepsilon_1\mu_1 = \varepsilon_3\mu_3 = 2.4649$, $\varepsilon_0\mu_0 = \varepsilon_2\mu_2 = \varepsilon_4\mu_4 = 2.4025$, and $\lambda = 1.3$ μm with respect to the point H as shown in Fig. 2.

the electrical field distribution with respect to the point B, as shown in Fig. 2. The points A and B on the same dispersion curve are mode 1. The numerical results show that when the guided power increases, the electric field distributions are gradually narrowed in the Kerr-type nonlinear NRI slab guiding films. The guided power will decrease sharply in the region of Kerr-type nonlinear interaction layer. Figure 5 shows the electrical field distribution with respect to the point C, as shown in Fig. 2. Figure 6 shows the electrical field distribution with respect to the point D, as shown in Fig. 2. Figure 7 shows the electrical field distribution with respect to the point E, as shown in Fig. 2. Figure 8 shows the electrical field distribution with respect to the point F, as shown in Fig. 2. The points C, D, E, and F on the same dispersion curve are mode 2. The numerical results show that when the guided power increases, the electric field distributions are gradually narrowed in the Kerr-type nonlinear NRI slab guiding films. The guided power will decrease in the region of Kerr-type nonlinear interaction layer. Figure 9 shows the electrical field distribution with respect to the point G, as shown in Fig. 2. Figure 10 shows the electrical field distribution with respect to the point H, as shown in Fig. 2. The points G and H on the same dispersion curve are mode 3. The numerical results show that when the guided power increases, the electric field distributions are gradually narrowed in the Kerr-type nonlinear NRI slab guiding films. The guided power will focus in the central region of Kerr-type nonlinear interaction layer. Figure 11 shows the electrical field distribution with respect to the point I, as shown in Fig. 2. Figure 12 shows the electrical field distribution with respect to the point J, as shown in Fig. 2. The points I and J on the same dispersion curve are mode 4. The numerical
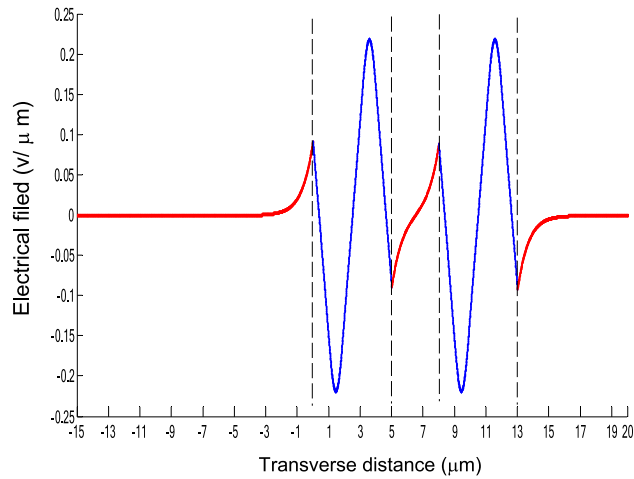
Figure 11. The electrical field distribution of the five-layer all Kerr-type nonlinear NRI slab optical waveguide structure with constants: $\alpha_0 = \alpha_1 = \alpha_2 = \alpha_3 = \alpha_4 = 6.3786 \ \mu m^2/V^2, \mu_f = \mu_1 = \mu_3 = -2$, $d_1 = d_3 = 5 \ \mu m, d_2 = 3 \ \mu m, \varepsilon_f \mu_f = \varepsilon_1 \mu_1 = \varepsilon_3 \mu_3 = 2.4649, \varepsilon_0 \mu_0 = \varepsilon_2 \mu_2 = \varepsilon_4 \mu_4 = 2.4025$, and $\lambda = 1.3 \ \mu m$ with respect to the point I as shown in Fig. 2.
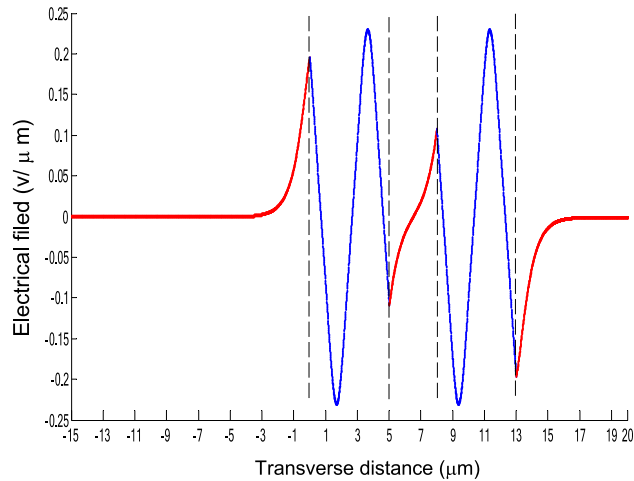

Figure 12. The electrical field distribution of the five-layer all Kerr-type nonlinear NRI slab optical waveguide structure with constants: $\alpha_0 = \alpha_1 = \alpha_2 = \alpha_3 = \alpha_4 = 6.3786 \ \mu m^2/V^2, \mu_f = \mu_1 = \mu_3 = -2$, $d_1 = d_3 = 5 \ \mu m, d_2 = 3 \ \mu m, \varepsilon_f \mu_f = \varepsilon_1 \mu_1 = \varepsilon_3 \mu_3 = 2.4649, \varepsilon_0 \mu_0 = \varepsilon_2 \mu_2 = \varepsilon_4 \mu_4 = 2.4025$, and $\lambda = 1.3 \ \mu m$ with respect to the point J as shown in Fig. 2.

results show that when the guided power increases, the electric field distributions are gradually narrowed in the Kerr-type nonlinear NRI slab guiding films. The guided power will increase in the region of Kerr-type nonlinear interaction layer. Figure 13 shows the electrical field distribution with respect to the point K, as shown in Fig. 2. Figure 14 shows the electrical field distribution with respect to the point L, as shown in Fig. 2. The points K and L on the same dispersion curve are mode 5. The numerical results show that when the guided power increases, the electric field distributions are gradually narrowed in the Kerr-type nonlinear NRI slab guiding films. The guided power will increase sharply in the region of Kerr-type nonlinear interaction layer.

The proposed general method can also be degenerated to study some special cases:

For case 1, the $\alpha_j = 0$, $j = 1, 3, 5...N-2$, and $\beta < \varepsilon_j \mu_j$, $A_j = q_j$, $\text{sn}\left[A_j x \big| m_j\right] = \sin(q_j x)$, $\text{cn}\left[A_j x \big| m_j\right] = \cos(q_j x)$, $\text{dn}\left[A_j x \big| m_j\right] = 1$, and the electric field of the Eq. (16) can be rewritten as:

$$E_j(x) = b_j cn\left[A_j\left(x + x_j\right)\big| m_j\right] = A_{f,i} \cos(q_j(x - x_j)), \text{ for } j = 1, 3, 5...N - 2 \tag{21}$$

For case 2, the $\alpha_j = 0$, $j = 1, 3, 5...N-2$, and $\beta > \varepsilon_j \mu_j$, $A_j^2 = Q_j^2 = -k_0^2(\varepsilon_j \mu_j - \beta^2)$, $\text{sn}\left[A_j x \big| m_j\right] = tanh(Q_j x)$, $\text{cn}\left[A_j x \big| m_j\right] = \sec h(Q_j x)$, $\text{dn}\left[A_j x \big| m_j\right] = sech(Q_j x)$, and the electric field of the Eq. (16) can be rewritten as:
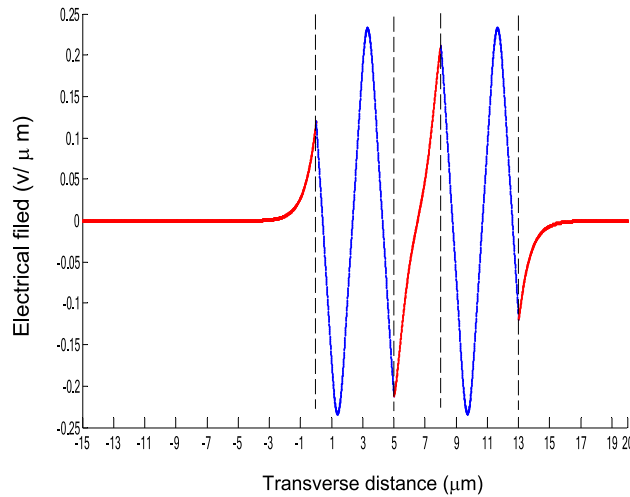
Figure 13. The electrical field distribution of the five-layer all Kerr-type nonlinear NRI slab optical waveguide structure with constants: $\alpha_0 = \alpha_1 = \alpha_2 = \alpha_3 = \alpha_4 = 6.3786 \ \mu\mathrm{m}^2/\mathrm{V}^2, \mu_f = \mu_1 = \mu_3 = -2, d_1 = d_3 = 5 \ \mu\mathrm{m}, d_2 = 3 \ \mu\mathrm{m}, \varepsilon_f\mu_f = \varepsilon_1\mu_1 = \varepsilon_3\mu_3 = 2.4649, \varepsilon_0\mu_0 = \varepsilon_2\mu_2 = \varepsilon_4\mu_4 = 2.4025,$ and $\lambda = 1.3 \ \mu\mathrm{m}$ with respect to the point K as shown in Fig. 2.
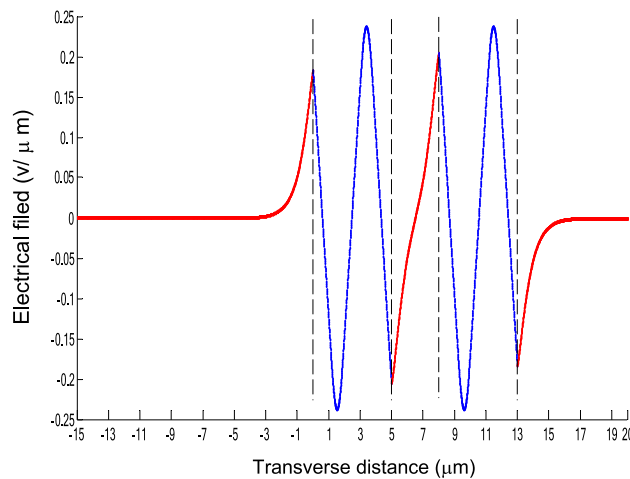

Figure 14. The electrical field distribution of the five-layer all Kerr-type nonlinear NRI slab optical waveguide structure with constants: $\alpha_0 = \alpha_1 = \alpha_2 = \alpha_3 = \alpha_4 = 6.3786 \ \mu\mathrm{m}^2/\mathrm{V}^2, \mu_f = \mu_1 = \mu_3 = -2, d_1 = d_3 = 5 \ \mu\mathrm{m}, d_2 = 3 \ \mu\mathrm{m}, \varepsilon_f\mu_f = \varepsilon_1\mu_1 = \varepsilon_3\mu_3 = 2.4649, \varepsilon_0\mu_0 = \varepsilon_2\mu_2 = \varepsilon_4\mu_4 = 2.4025,$ and $\lambda = 1.3 \ \mu\mathrm{m}$ with respect to the point L as shown in Fig. 2.

$$E_j(x) = b_j cn\left[A_j\left(x + x_j\right)\big|m_j\right] = A_{f,i}\cosh(Q_j\left(x - x_j\right)) \ \text{ for j} = 1, 3, 5... \ \mathrm{N} - 2 \tag{22}$$

For case 3, the parameters $\alpha_{\mathrm{N}-1} = 0$ and $B_c = 1$, the electric field in the nonlinear DPS cladding $E_{\mathrm{N}-1}$ can be expressed as:

$$E_j(x) = E_j\left\{\cosh[q_j(x - x_{\mathrm{N}-1})] + B_c \sinh[q_j(x - x_{\mathrm{N}-1})]\right\}^{-1} = A_c \exp(-q_j x) \ \text{ for j} = \mathrm{N} - 1 \tag{23}$$

For case 4, the parameters $\alpha_0 = 0$ and $B_s = 1$, the electric field in nonlinear the substrate E_s can be written as:

$$E_0(x) = E_1\left\{\cosh(q_0 x) - B_s \sinh(q_0 x)\right\}^{-1} = A_s \exp(q_0 x) \tag{24}$$

The Eqs. (21)–(24) can be used to drive some degenerated examples of the NRI multilayer slab optical waveguide structures. The numerical results are same to that of the previous papers[59,60]. It showed that the proposed general method can be degenerated into any kind of the NRI multilayer slab optical waveguide structures. The relative parameters are shown in Online Appendix I–III.

Conclusions

In this paper, we proposed a general method for analyzing arbitrary NRI multilayer slab optical waveguide structures. This general method can simultaneously be used to degenerate into different kinds of NRI multilayer slab waveguide structures by properly varying the nonlinear coefficient. Some degenerated examples were introduced to prove the accuracy of the proposed method. The analytical and numerical results show excellent agreement. The method can also be degenerated to analyze arbitrary planar conventional optical waveguide structures. Based on this general method, the analysis and calculation of any kinds of NRI multilayer slab optical waveguide structures and conventional multilayer slab optical waveguide structures can be achieved easily.

References

1. Shelby, R. A., Smith, D. R. & Schultz, S. Experimental verification of a negative index of refraction. *Science* **292**(5514), 77–79 (2001).
2. Veselago, V. G. The electrodynamics of substances with simultaneously negative values of ε and μ. *Sov. Phys. Usp.* **10**(4), 509–514 (1968).
3. Ziolkowski, R. W. & Heyman, E. Wave propagation in media having negative permittivity and permeability. *Rev. E.* **64**, 056625 (2001).
4. Milonni, P. W. & Maclay, G. J. Quantized-field description of light negative-index media. *Opt. Commun.* **228**, 161–165 (2003).
5. Castaldi, G., Gallina, I., Galdi, V., Alú, A. & Engheta, N. Cloak/anti-cloak interactions. *Opt. Express* **17**, 3101–3114 (2009).
6. Awad, M., Nagel, M. & Kurz, H. Negative-index metamaterial with polymer-embedded wire-pair structures at terahertz frequencies. *Opt. Lett.* **33**, 2683–2685 (2008).
7. Duan, Z. Y., Wu, B. I., Xi, S., Chen, H. & Chen, M. Research progress in reversed Cherenkov radiation in double-negative metamaterials. *Prog. Electromagn. Res.* **90**, 75–87 (2009).
8. Xi, S., Chen, H., Wu, B. I. & Kong, J. A. Experimental confirmation of guidance properties using planar anisotropic left-handed metamaterial slabs based on S-ring resonators. *Prog. Electromagn. Res.* **84**, 279–287 (2008).
9. Wu, W.-Y., Lai, A., Kuo, C. W., Leong, K. M. K. H. & Itoh, T. Efficient FDTD method for analysis of mushroom-structure based left-handed materials. *IET Microwaves Antennas Propag.* **1**, 100–107 (2007).
10. Dolling, G., Wegener, M., Soukoulis, C. M. & Linden, S. Negative-index metamaterial at 780 nm wavelength. *Opt. Lett.* **32**, 53–55 (2007).
11. Yu, G. X. *et al.* Transformation of different kinds of electromagnetic waves using metamaterials. *J. Electromagn. Waves Appl.* **23**(5), 583–592 (2009).
12. Zhou, H. *et al.* A planar zero-index metamaterial for directive emission. *J. Electromagn. Waves Appl.* **23**, 953–962 (2009).
13. Gong, Y. & Wang, G. Superficial tumor hyperthermia with flat left-handed metamaterial lens. *Prog. Electromagn. Res.* **98**, 389–405 (2009).
14. Wang, M.-Y. *et al.* FDTD study on wave propagation in layered structures with biaxial anisotropic metamaterials. *Prog. Electromagn. Res.* **81**, 253–265 (2008).
15. Zhang, J., Luo, Y., Chen, H. & Wu, B. I. Efficient complementary metamaterial element for waveguide fed metasurface antennas. *Opt. Express* **25**, 28686–28692 (2016).
16. Segovia, P. *et al.* Hyperbolic metamaterial antenna for secondharmonic harmonic generation tomography. *Opt. Express* **23**, 30730–30738 (2015).
17. Landy, N. I., Sajuyigbe, S., Mock, J. J., Smith, D. R. & Padilla, W. J. Perfect metamaterial absorber. *Phys. Rev. Lett.* **100**, 207402 (2008).
18. Alaee, R. *et al.* Perfect absorbers on curved surfaces and their potential applications. *Opt. Express* **20**, 18370–18376 (2012).
19. Jang, Y., Yoo, M. & Lim, S. Conformal metamaterial absorber for curved surface. *Opt. Express* **21**, 24163–24170 (2013).
20. Liu, N. *et al.* Infrared perfect absorber and its application as plasmonic sensor. *Nano Lett.* **10**, 2342–2348 (2010).
21. Yi, C. *et al.* Analysis of a systematic error appearing as a periodic in the frequency-domain absorption spectra of metamaterial absorbers. *Opt. Express* **25**, 13296–13304 (2017).
22. Capecchi, W. J., Behdad, N. & Volpe, F. A. Reverse chromatic aberration and its numerical optimization in a metamaterial lens. *Opt. Express* **20**, 8761–8769 (2012).
23. Orazbayev, B., Pacheco-Peña, V., Beruete, M. & Navarro-Cía, M. Exploiting the dispersion of the double-negative index fishnet material to creat a broadband low-profile metallic lens. *Opt. Express* **23**, 8555–8564 (2015).
24. Islam, S. S., Faruque, M. R. I. & Islam, M. T. A near zero refractive index metamaterial for electromagnetic invisibility cloaking operation. *Materials* **8**, 4790–4804 (2015).
25. Guenneau, S., Petiteau, D., Zerrad, M. & Amra, C. Bicephalous transformed media concentrator versus and cloak versus superscatterer. *Opt. Express* **22**, 23614–23619 (2014).
26. Vrba, J. & Vrba, D. A microwave metamaterial inspired sensor for non-invasive blood glucose monitoring. *Radioengineering* **24**, 877–884 (2015).
27. Sarwadnya, R. R. & Dawande, N. A. Literature review of metamaterial based sensing devices. *IJIRSET* **5**, 19028–19031 (2016).
28. Taya, S. A., Shabat, M. M. & Khalil, H. M. Enhancement of sensitivity in optical waveguide sensors using left-handed materials. *Optik* **120**, 504–508 (2009).
29. S. A. Taya, E. J. El-Farram, T. M. El-Agez. Goos–Hanchen shift as a probe in evanescent slab waveguide sensors. Int. J. Electron. Commun. **66**, 204–210 (2012).
30. Chen, H. T. *et al.* A metamaterial solid-state terahertz phase modulator. *Nat. Photonics* **3**, 148–151 (2009).
31. Yan, R., Sensale-Rodriguez, B., Liu, L., Jena, D. & Xing, H. G. (2012) A new class of electrically tunable metamaterial terahertz modulators. *Opt. Express* **20**(27), 28664–28671 (2012).
32. Larouche, S., Tsai, Y. J., Tyler, T., Jokerst, N. M. & Smith, D. R. Infrared metamaterial phase holograms. *Nat. Mater.* **11**, 450–454 (2012).
33. Lipworth, G., Caira, N. W., Larouche, S. & Smith, D. R. Phase and magnitude constrained metasurface holography at W-band frequencies. *Opt. Express* **24**, 19372–19387 (2016).
34. Manapati, M. B. & Kshetrimayum, R. S. SAR reduction in human head from mobile phone radiation using single negative metamaterials. *J. Electromag. Waves Appl.* **23**(10), 1385–1395 (2009).
35. Hwang, R.-B., Liu, H.-W. & Chin, C.-Y. A metamaterial-based E-plane horn antenna. *Prog. Electromagn. Res.* **93**, 275–289 (2009).
36. Huang, M. D. & Tan, S. Y. Efficient electrically small prolate spheroidal antennas coated with a shell of double-negative metamaterials. *Prog. Electromagn. Res.* **82**, 241–255 (2008).
37. Si, L.-M. & Lv, X. CPW-FED multi-band omni-directional planar microstrip antenna using composite metamaterial resonators for wireless communications. *Prog. Electromagn. Res.* **83**, 133–146 (2008).

38. Al-Naib, A. I., Jansen, C. & Koch, M. Single metal layer CPW metamaterial band-pass filter. *Prog. Electromagn. Res. Lett.* **17**, 153–161 (2010).
39. Mirza, O., Sabas, J. N., Shi, S. & Prather, D. W. Experimental demonstration of metamaterial based phase modulation. *Prog. Electromagn. Res.* **93**, 1–12 (2009).
40. Sabah, C. & Uckun, S. Multilayer system of Lorentz/drude type metamaterials with dielectric slabs and its application to electromagnetic filters. *Prog. Electromagn. Res.* **91**, 349–364 (2009).
41. Wu, Y. D. New all-optical switch based on the spatial soliton repulsion. *Opt. Express.* **14**, 4005 (2006).
42. Wu, Y. D., Whang, M. L., Chen, M. H. & Tasy, R. Z. All-optical switch based on the local nonlinear Mach-Zehnder interferometer. *Opt. Express.* **15**, 9883 (2007).
43. Wu, Y. D. All-optical logic gates by using multibranch waveguide structure with localized optical nonlinearity. *IEEE J. Sel. Top. Quantum. Electron.* **11**, 307 (2005).
44. Wu, Y. D., Huang, M. L., Chen, M. H. & Tasy, R. Z. All-optical switch based on the local nonlinear Mach-Zehnder interferometer. *Opt. Express* **15**, 9883–9892 (2007).
45. Wu, Y. D., Shih, T. T. & Chen, M. H. New all-optical logic gates based on the local nonlinear Mach-Zehnder interferometer. *Opt. Express* **16**, 248–257 (2008).
46. Kaman, V. *et al.* A 32 × 10 Gb/s DWDM metropolitan network demonstration using wavelength-selective photonic cross-connects and narrow-band EDFAs. *IEEE Photonics Technol. Lett.* **17**, 1977–1979 (2005).
47. Shadrivov, V., Sukhorukov, A. A. & Kivshar, Y. S. Guided modes in negative-refractive-index waveguides. *Phys. Rev. E* **67**, 057602 (2003).
48. Darmanyan, S. A., Nevière, M. & Zakhidov, A. A. Nonlinear surface waves at the interfaces of left-handed electromagnetic media. *Phys. Rev. E* **72**, 036615 (2005).
49. Ziolkowski, R. W. & Heyman, E. Wave propagation in media having negative permittivity and permeability. *Phys. Rev. E* **64**, 056625 (2001).
50. Shadrivov, V. *et al.* Nonlinear surface waves in left-handed materials. *Phys. Rev. E* **69**, 016617 (2004).
51. Shen, M., Ruan, L. & Chen, X. Guided modes near the dirac point in negative-zero-positive index metamaterial waveguide. *Opt. Express* **18**(127), 12779–12787 (2010).
52. He, J., He, Y. & Hong, Z. Backward coupling of modes in a left-handed metamaterial tapered waveguide. *IEEE Microw. Wirel. Compon. Lett* **20**(7), 378–380 (2010).
53. Pollock, J. G. & Iyer, A. K. Below-cutoff propagation in metamaterial-lined circular waveguides. *IEEE Trans. Microw Theory Techn.* **61**(9), 3169–3178 (2013).
54. Duan, Z., Wu, B.-I., Lu, J., Kong, J. A. & Chen, M. Cherenkov radiation in anisotropic double-negative metamaterials. *Opt. Express* **16**(22), 18479–18484 (2008).
55. Duan, Z. *et al.* Observation of the reversed Cherenkov radiation. *Nat. Commun.* **8**, 14901 (2017).
56. Wu, Y. D. & Cheng, M. H. Analyzing the multilayer metamaterial waveguidestructure with the Kerr-type nonlinear cladding. *Opt. Quant. Electron* **49**, 1–18 (2017).
57. Chilwell, J. & Hodgkinson, I. Thin-films field-transfer matrix theory of planar multilayer waveguides and reflection from prism-loaded waveguides. *J. Opt. Soc. Amer. A* **1**, 742–753 (1984).
58. Doer, C. R. & Kogelnik, H. Dielectric waveguide theory. *J. Lightwave Technol.* **26**, 1176–1187 (2008).
59. Kuo, C. W., Chen, S. Y., Wu, Y. D., Chen, M. H. & Chang, C. F. Analysis and calculations of forbidden regions for transverseelectric-guided waves in the three-layer planar waveguide with photonic metamaterial. *Fiber Integr. Opt.* **29**, 305–314 (2010).
60. Kuo, C. W., Chen, S. Y., Wu, Y. D. & Chen, M. H. Analyzing the multilayer optical planar waveguides with double-negative metamaterial. *Prog. Electricmagn. Res.* **110**, 163–178 (2010).

Acknowledgements

Author contributions
Y.-D.W. is responsible for the whole manuscript.

Competing interests
The author declares no competing interests.

Additional information
Supplementary information is available for this paper at https://doi.org/10.1038/s41598-020-72017-3.

Correspondence and requests for materials should be addressed to Y.-D.W.

Reprints and permissions information is available at www.nature.com/reprints.

Publisher's note Springer Nature remains neutral with regard to jurisdictional claims in published maps and institutional affiliations.